Original article

CONDITION ASSESSMENT OF THE OSIRIS CHAPEL WALL PAINTINGS IN SETI-I TEMPLE, ABYDOS - EGYPT

Motawea, A-G[1][(*)], El-Hossary, F.[2] & El-Gohary, M.[3]

[1]*Conservation dept., Ministry of Tourism and Antiquities, Sohag, Egypt*
[2]*Physics dept., Faculty of Science, Sohag Univ., Sohag, Egypt.*
[3]*Conservation dept., Faculty of Archaeology, Zagazig Univ., Zagazig, Egypt.*
E-mail address: tantawe2009_fm@yahoo.com

Abstract:
This paper describes the condition of the painted decorations in Osiris chapel and identifies their original materials and implementation techniques by studying the stratigraphic structure. It includes information on the accumulation of soot layers as the most effective deterioration factor in the chapel. In addition, it assesses and documents the condition. Investigations were carried out using optical microscopy (OM), scanning electron microscopy coupled with energy-dispersive X-ray spectroscopy (SEM-EDX), X-ray diffraction (XRD), and attenuated total reflection-Fourier transform infrared (ATR-FTIR) spectroscopy. The results indicated that the blue pigment revealed Egyptian blue (Cuprorivaite), the green pigment was Egyptian green, the red pigment was red ochre, and the yellow pigment was yellow ochre. Furthermore, the used plaster layer is consisted of gypsum, the vaulted ceiling is constructed by sandstone, and the walls were built from fine crystalline limestone. The accumulated soot was noticed as black particles under the optical microscope, which showed as dark gray composed of graphite according to XRD that was composed of carbon as EDX result and graphite according to XRD. The hydrophobic coatings in the presence of external agents could trigger multiple deterioration mechanisms. The documentation of the wall paintings' condition was done via Autocad and Photoshop layers.

1. Introduction

Abydos is one of the oldest centers of civilization in Upper Egypt [1], located about 300 miles south of Cairo. It contains many important relics places and archaeological buildings, such as the Temple of Seti I and Ramssis II Temple. Seti I temple, fig. (1-a), was built by Seti I in the 19th dynasty (1293-1185 BC) [2] and was completed after his death by his son Ramssis II [3]. The temple stone reliefs are some of the finest and most delicate in any Egyptian temple. Moreover, the temple is an "L" shaped design, and it

has a terrace, multiple courts and chambers, two pylons, and seven chapels dedicated to Seti I and ancient gods, fig. (1-b) [4,5]. In the current study, one of the most important chapels in the temple (*Osiris Chapel*) was studied. It is a rectangular room extending from east to west by about 10 m^2 and from north to south by about 5 m^2 and is covered by a vaulted ceiling along its length [6]. The decorations in this chapel are in good preservation condition and were executed with great precision and craftsmanship. The

old artisan used limestone to construct the walls, while the vaulted ceiling was built from sandstone. The chapel was decorated with high precision sunk/raised reliefs. Then, red, yellow, blue, green, and black pigments were used to color these reliefs. The distribution of pigments in the ceiling was identified through repeated relief figures, which were not completely obscured by soot [7]. The chapel contains a group of very impressive décorations and inscriptions for the king and his daily activities, such as kneeling and offering necklaces to Osiris [8,9]. Furthermore, the vaulted ceiling was decorated with prominent and repeated carvings of stars and cartouche, which bore the royal title for King Seti: "Menmaetre" [10]. Most of the inscriptions in this hall were executed during the reign of king Seti I. They are very exquisite inscriptions that retain their luster even now. The scenes prevailing in most of the chapels are the scenes of offerings directed toward the individual gods and depictions of skiffs housing the divine images [11]. From a conservation point of view, few studies were conducted on the condition assessment of decorations and their deterioration aspects in the Seti I temple, e.g. [2,3,12,13]. In this regard, the present study is considered the first on the condition assessment of painted decorations in this chapel to identify the extent of its depth in the ancient painted surface.
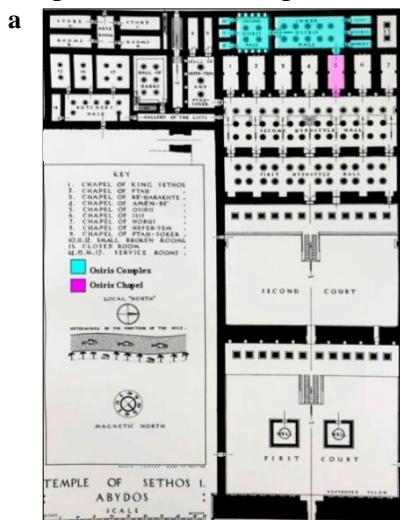

Figure (1) Shows **a.** the plan of the temple, **b.** general view of the temple

2. Condition Assessment

The decay of the building materials, such as stones, bricks, mortars, and paintings, is a complex phenomenon [14]. It occurs through various deterioration mechanisms mostly due to external and internal deterioration factors and related mechanisms that create different deterioration forms [15,16]. The main objective of this section is to assess the harmful effects of painted decorations in the *Osiris chapel and Seti I temple*. These influences are attributed essentially to some unwanted materials, e.g., *soot accumulations* and *acrylic coatings,* as human effects [17]. In this regard, a documentation system was designed to show the different deterioration of two previous aspects, including:

1) A photograph coupled with a scale for the current condition before treatment. **2)** Using Photoshop program to draw the details of reliefs. **3)** Taking three copies of the basic drawing highlighting the dispersions of the deterioration aspects of the figurative layer, the preparatory and supporting layer, and the locations of the treatments already performed. All these features are shown in figs. (2 & 3).
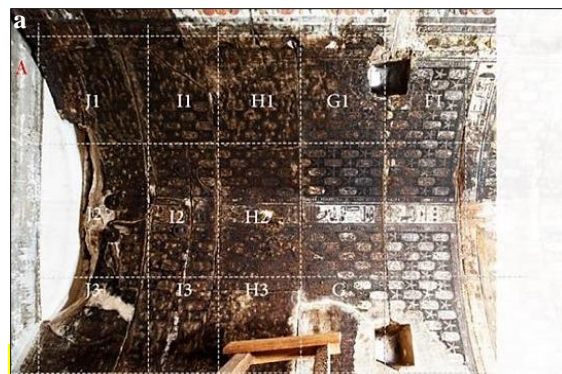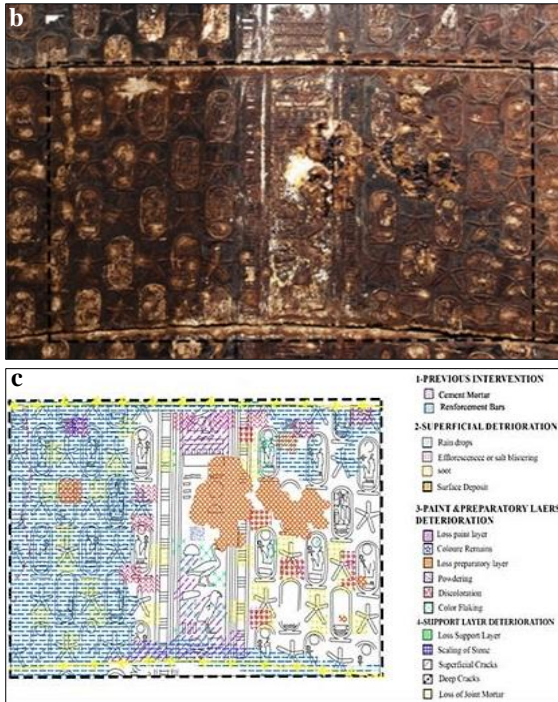
Figure (2) Shows **a**. panoramic view of the ceiling divide from (A-J) plats, **b**. sample of ceiling documentation, **c**. layers after combining.
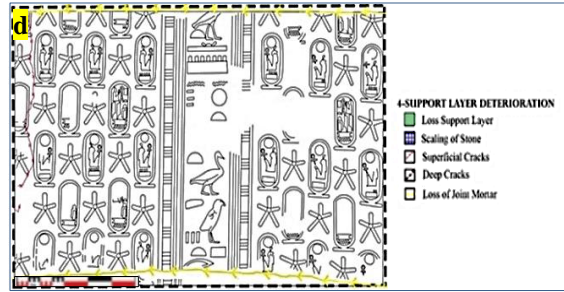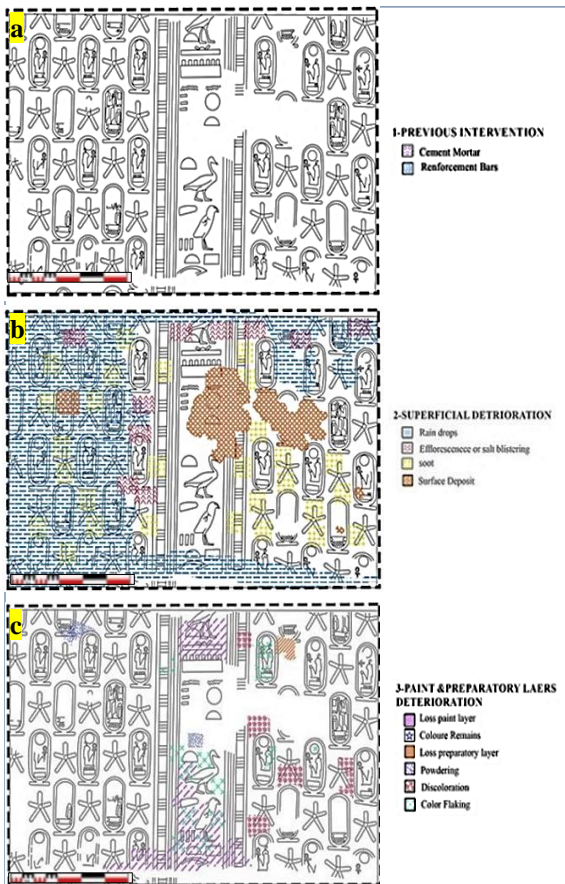

Figure (3) Shows **a.** layer 1 of documentation with previous intervention in H2 plate, **b.** layer 2 superficial deterioration, **c.** layer 3 deterioration aspects of paint and preparatory, **d.** layer 4 deterioration aspects of support layer.

2.1. *Soot accumulations*

The ceiling of the chapel suffers from the accumulation of *soot layers*, which led to the obliteration of the decorations with soot. Christian monks used these places as safe havens and shelters [3,7]. Thus, they used fire for various purposes, such as cooking and lighting [18]. The dense soot concentrated over the ceiling area and the curves directly below it. As for the walls, the accumulation of soot was less. The distribution of pigments in the ceiling was identified through repeated figures, which were not completely obscured. Soot is composed of an oily tarry matrix mixed with carbon to form a blackened oily film [19]. During the fire, the soot particles separate in the air due to their weight; the larger particles agglomerate dropping out of the air closest to the fire, and the finer particles agglomerate farther from the fire [20]. The electrostatic attraction phenomenon is the main reason for the stability of soot particles on surfaces, which penetrate the finest holes of the porous surface and adhere to the surface [21,22]. Over time, fine soot particles become embedded in painted surfaces due to penetrating interstices [23]. The accumulation of soot causes significant visual changes to decorations, obscuring the details of the artistic and aesthetic values of these monuments by soiling [24,25]. In addition, it changes the water permeability properties of the original surface [26]. Soot

contains acidic components causing the decay of the stone [24]. Soot and other organic compounds form a suitable medium for SO_2 absorption from atmospheric air, and these effects increase by $CaSO_4$ [27].

2.2. Acrylic coatings

Through previous periods, many hydrophobic coatings were applied for the consolidation and protection of painted decorations [28]. These resins have been used in the preservation of antiquities since the 1960s [29]. One of the most widely used consolidation and protection acrylic-based products is methyl acrylate/ethyl methacrylate (MA/EMA) copolymer [30]. It is well known for its good adhesive power, transparency, and solubility in several solvents [31]. Over time, they are susceptible to degradation due to different external agents, such as temperature, moisture, salts, light, microorganisms, etc. Those agents can trigger multiple deterioration mechanisms, damaging one or more strata of the wall painting [32]. Although these polymers served their intended purpose, they still threaten the paintings' stability because they obstruct the surface pores and prevent the movement of internal moisture and air, "preventing the stone from breathing" [33]. However, some limitations have been noticed through various studies undertaken over long years of usage, like poor penetration into porous and non-porous stones, reduced reversibility of aged polymer, and lower hydro repellency in comparison to silicone polymers [34]. In our case, the use of these polymers led to the trapping of liquids inside, as they are hydrophobic and incompatible with inorganic porous surfaces [35], specialty with the high thickness that was shown clearly fig. (3). It further exacerbated the damage to painted surfaces, and thus increased the complexity of the deterioration state, especially the presence of chromatic variations [36].

3. Materials and Methods

3.1. Materials

Different samples of ancient painted decorations (i.e., *limestone, sandstone, plaster,*

mortar, and *pigments*) have been collected from the Osiris chapel. Moreover, some contaminated samples with soot and some other samples protected with acrylic coatings were also collected to be targeted for the following investigation.

3.2. Methods

The paint samples were examined visually via digital photos that were taken by a high-quality professional digital camera (model: *Nikon D7200 N1406, 24.2 megapixels, with lens AF-S Nikkor 18-104 mm^2*) and an external flash (SB-700). The cross-sections, pigments, and soot, as well as extending soot overlapping with the pigment granules, were observed by OLYMPUS Stream™ optical microscope (*model BX51 and software V. 2.4.2*) provided with a digital camera (*model Dp70*) that captured the live images for the exposed surface. Scanning electronic microscopy (SEM) equipped with a secondary electrons detector–and energy dispersive X-ray analysis (EDX) was used to determine the morphology and elemental chemical composition of pigments, plaster, stones, and soot. SEM (*model was a Quanta 250 FEG with an acceleration voltage of 20 kV and 1×10^{-9} A, and an EDAX/DX4 detector, at a working distance of 10 mm. The specimens were coated by an extremely thin layer of gold (1.5-3 nm) using a sputter coater machine*). Furthermore, a *Bruker D8 XRD instrument* was used to identify the accumulated soot, pigments, plaster layers, and stones. The X-ray source of a closed copper tube produces Cu kα radiation with wavelength 1.5406 Å from a generator operating at 40 kV and 40 mA. A parallel beam of monochromatic X-ray radiation is produced using a Göbel mirror optic (primary optic). The beam impingement angle started at 10^0 to 80^0 relative to the sample's surface. Finally, a *Bruker ALPHA FTIR spectrometer with an ATR correction method featuring a single-bounce diamond ATR* was also employed. The measurements were recorded in the region (4000-

400 cm^{-1}) with a spectral resolution of 4 cm^{-1} [37]. This technique provided a quick analysis to identify the accumulation of soot, pigments, stones, and plaster. In addition, it showed any changes that might occur to the binding medium [38].

4. Results
4.1. *Deterioration features*
4.1.1. Soot layer

Visually, a very thick layer of accumulated soot was concentrated on the ceiling, fig. (4-a) due to the fire point, while it decreased on both sides in the downward direction of the walls, fig. (4-b). Furthermore, the soot layer was strongly bonded to the surface due to the high ratio of limestone. It was shown as semicircle grey granules under the optical microscope with a thick cracked layer on the ceiling, and its black deposits on the walls, fig. (4-c). Morphologically, the same layer varied between white to gray particles in SEM photogrammetric composed essentially of carbon (C), fig. (4-d & e). Additionally, it appeared in XRD analysis as a major mineral in the sample taken from the ceiling, while the minor mineral in the sample taken from the walls, fig. (4-f). Even more, the same layer through ATR-FTIR analysis appeared as CH2 asymmetric vibration peak at 2970 cm^{-1}, as well as the characteristic peaks in the region 3000-2800 cm^{-1}(62). The most significant single peaks at 1740 and 1738 cm^{-1} showed ester (C=O) stretching vibration bands specific to the oil carbon soot. In addition, the peaks in the region 1440-1070 cm^{-1} indicated (C-O) stretching bond that represents ethers, carboxylic acids, and polysaccharide, fig. (4-g).
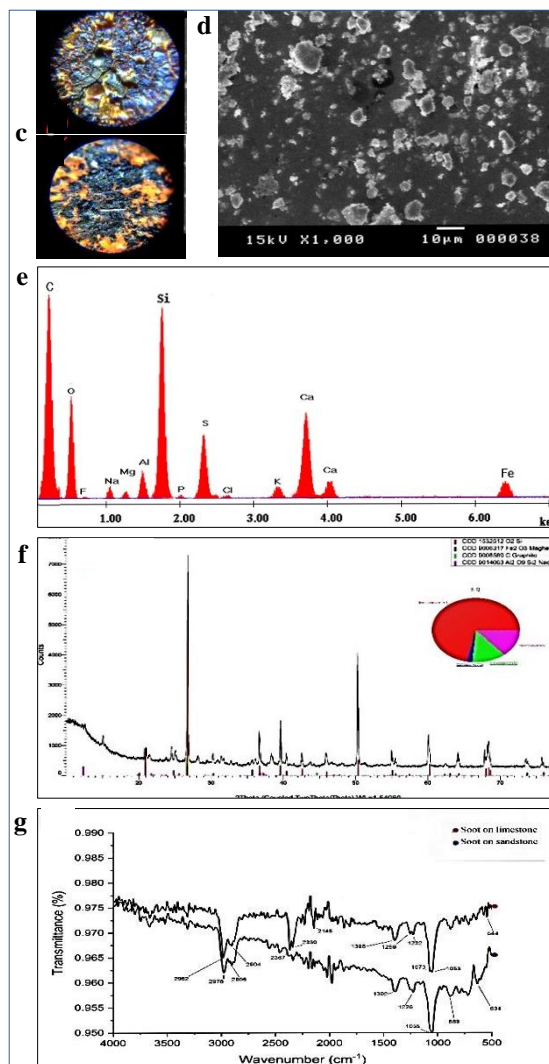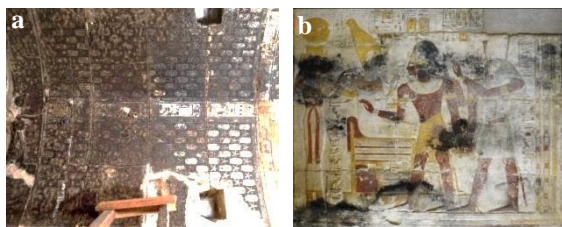

Figure (4) Shows **a.** overview for the ceiling obliterated with accumulation soot layers, **b.** the walls stained with less soot, **c.** confirming two cases via optical microscope, **d.** SEM photomicrograph of the soot particles on the painted surface, **e.** EDX elemental analysis with high carbon content, **f.** XRD pattern of soot with presence of graphite (C), besides the nacrit (Al$_2$O$_9$Si$_2$), and maghemite (Fe$_2$O$_3$), **g.** FTIR spectra of soot on the ceiling and walls.

4.1.2. Acrylic coatings

Regarding the visual and microscopic examinations, fig. (5-a) shiny appearance of the paints could be noted, in addition to some cracks in the coating material that appeared after drying, fig. (5-b). Furthermore, changing the optical appearance of painted surfaces (which became yellowish and/or darkened)

due to their high refractive index, especially when used with high concentrations, led finally to a photochemical degradation process, fig. (5-c & d). XRD analysis showed that the polymer appeared in a significantly rising main peak, fig. (5-e). This peak pointed to *polyvinyl alcohol* as the most famous coating during this period. For the aforementioned reasons, conservation scientists believe that these coatings should be removed while preserving the original painted surfaces as much as possible. ATR-FTIR spectrum, fig. (5-f) was identified by the most prominent characteristic peaks at the region 1700-1300 cm^{-1} due to the carbonyl stretching vibration of the ester group. Besides, 1014, 979, and 875 cm$^{-1,}$ respectively, were from the asymmetric and symmetric C-O stretching of the ester group. Further diagnostic peaks were in the range of aliphatic chain stretching vibration (CH2- stretching at 2981 and 2906 cm^{-1}).
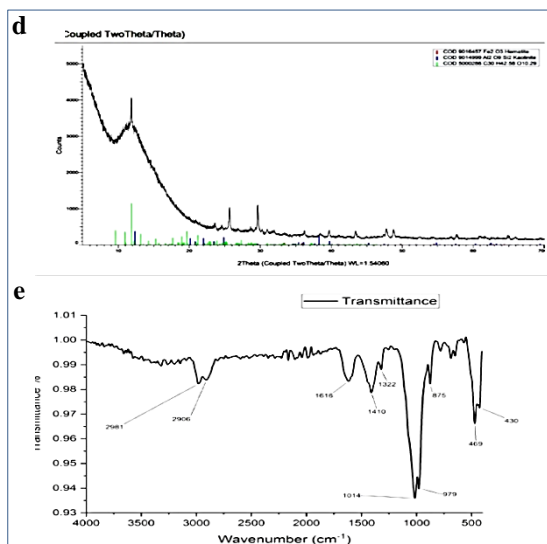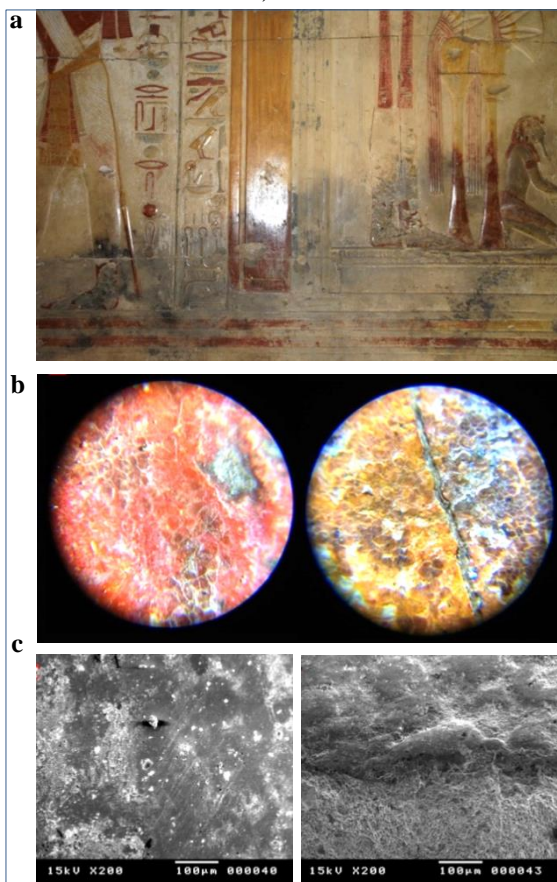

Figure (5) Shows **a.** shiny optical appearance of painted decorations caused by the acrylic coating, **b.** chemical decay of the consolidant in yellowish and/or darken features, **c.** shiny appearance with high thickness of consolidant as noticed in **d.** FTIR spectra of acrylic resin analysis, **e.** XRD pattern of acrylic resin as noticed a main peak that rises remarkably.

4.2. *Stratigraphy and technique*

Optical micrographs of the cross-section of the ceiling paint from the superficial to the innards parts, fig. (6-a) exhibited the following: **1)** 1st layer layer was the support composed of sandstone. **2)** 2nd layer was the plaster (~2-4 mm). **3)** 3rd was a paint with 100-150 μm thick. On the other hand, the cross-section of the wall painting showed that the thickness of the paint layer (70-100 μm) and the plaster were characterized by a very thin layer (600-1000 μm). SEM backscattered images showed that the ceiling paint consisted of a paint layer, a layer of gypsum, and a support from sub-rounded and angular quartz particles, fig. (6-b).
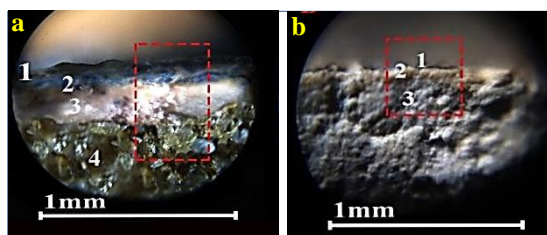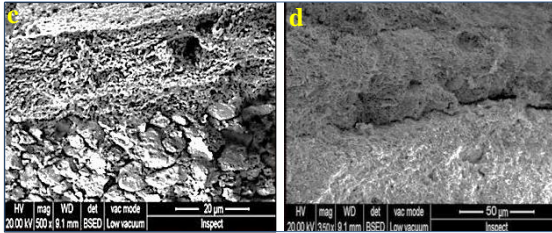
Figure (6) Shows the stratigraphy of **a.** the painted ceiling, **b.** the painted wall, **c. & d.** SEM morphological features of the same samples

4.2.1. Supports
4.2.1.1. *Limestone*

SEM micrographs, fig. (7-a) disclosed that the limestone sample contained a homogenyeous fine-crystalline structure composed of calcite matrix and dolomite. EDX analysis, fig. (7-b), revealed that the sample was mainly composed of (Ca, C, O, Si, & Mg), referred to as limestone. XRD analysis, fig. (7-c), correlated with the EDX analysis; thus, it denoted the main minerals calcite ($CaCO_3$), quartz (SiO_2), and ankerite ($Ca_{.997}$ ($Mg_{.273}$ $Fe_{.676}$ $Mn_{.054}$)(CO_3)$_2$). The ATR-FTIR spectrum of the limestone sample, fig. (7-d), displayed the characteristic carbonate bands, carbonyl C=O, and carbonate CO_3, respectively, at (1404, 873, and 675 cm^{-1}) and the symmetric characteristic bands at 1051 and 675 cm^{-1} denoted to Si-O-Si and Si-O, respectively.
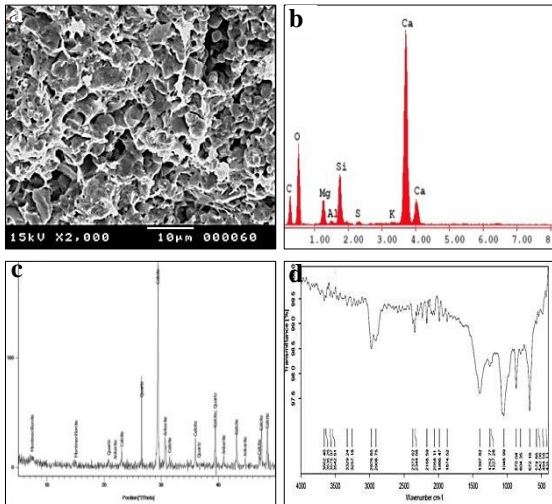

Figure (7) Shows **a.** SEM photomicrograph has calcite micrograins. **b.** EDX, **c.** XRD pattern with calcite & quartz of lime-stone (*main minerals*)**, d.** ATR-FTIR spectrum for limestone.

4.2.1.2. *Sandstone*

SEM photomicrographs, fig. (8-a) showed large-sized Qz granules with minor amounts of calcite and gypsum. EDX analysis, fig. (8-b) exhibited that sandstone samples were mainly composed of Si, O, in the presence of Al, K, Na, or Fe (*as components of cement materials*). XRD analysis of the mineral component, fig. (8-c), showed that the sandstone samples were composed mainly of quartz (SiO_2). In addition to anhydrite ($CaSO_4$) and kaolinite Al_2 (Si_2O_5)(OH)$_4$, this sample contained an amount of halite (NaCl), one of the deterioration aspects. FTIR-ATR spectrum, fig. (8-d) exhibited that the symmetrical bands at 996, 909, and 790 cm^{-1} correspond to Si-O symmetrical bending vibration. In addition, the other bands at 687, 530, and 459 cm^{-1} were compatible with Si–O–Si symmetrical and asymmetrical bending, respectively.
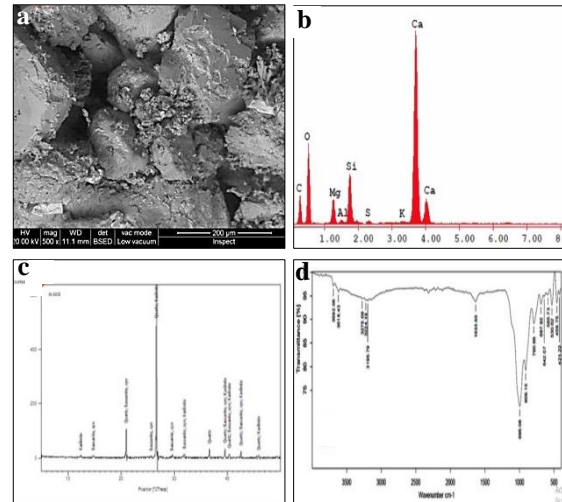
Figure (8) Shows **a.** SEM photomicrograph of sub-angular and rounded quartz grains and gypsum crystals as a cement material. **b.** EDX, **c.** XRD analysis of sandstone with *quartz & basanite* (*main mine-rals*)**, d.** ATR-FTIR spectrum for the sandstone.

4.2.2. Mortar and plaster

SEM photomicrographs of these components showed quartz as regular white crystals with regular edges, gypsum in white crystals like needles, and calcite as either white slaps with organized edges or spherical granules, fig. (9-a). EDX elemental and XRD mineralogical

analyses, fig. (9-b & c) were compatible. Thus, the high concentration of the elements (Ca, S, O, Si, and C) represented quartz (SiO_2), gypsum ($CaSO_4\ H_2O$), anhydrite ($CaSO_4$), and calcite in the plaster layer. Furthermore, the FTIR-ATR spectrum of the plaster, fig. (9-d) revealed carbonyl (C=O) absorption bands at 1722-1650 cm^{-1}, carbonate (-CO$_3$=) broad stretching band near 1433, 874, and 711 cm^{-1} referred to calcite in the plaster and the typical absorption band of gypsum at 1620 cm^{-1}. In addition, a strong sulfate S-O stretching vibration band was in the region of 1147 cm^{-1}. The strong stretching vibration bands were at 1101, 1028, and 1014 cm^{-1}, and the characteristic peaks at the region 675-466 cm^{-1} revealed the presence of silicate Si-O-Si.
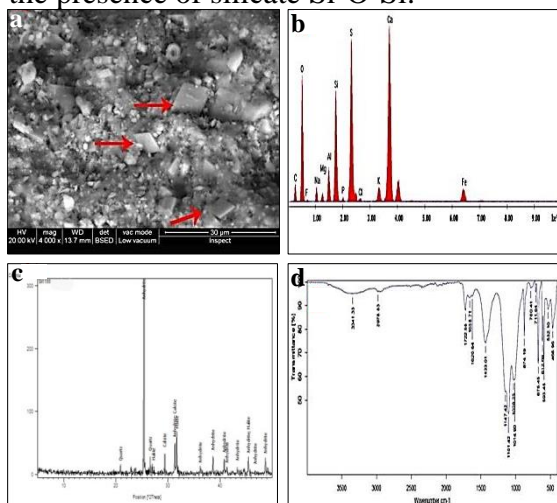

Figure (9) Shows **a.** SEM photomicrograph of different micrometric grains of calcite, quartz and gypsum, **b.** EDX, **c.** XRD patterns of joint mortar with anhydrate, quartz (*main minerals*) with (*halite*) as a trace, **c.** ATR-FTIR spectrum for the mortar or plaster.

4.2.3. Pigments
4.2.3.1. *Egyptian blue*
Egyptian blue is crystals like the fractions of glass as exhibited in optical microscope micrographs. SEM photomicrograph, fig. (10-a) provided a characteristic microstructure of such aggregates composed of polycrystalline material and silica granules. EDX patterns, fig. (10-b) presented the main elements, i.e.,

Ca, Si, Cu, O, and C. This mixture produced calcium-copper tetra silicate crystals (*Cuprorivaite*). XRD analytical results, fig. (10-c) referred that both quartz (SiO_2) and cuprorivaite ($CaCuO_{10}Si_4$) are the main minor minerals of Egyptian blue, and kyanite (Al_2O_5Si) is related to accumulated dust on the paint surface. Finally, FTIR-ATR spectrum of Egyptian blue, fig. (10-d), is distinct by the characteristic bands of silicates at 1059 cm^{-1} attributed to Si-O-Si stretching vibrations. Then, weak broad bands of calcite (C–O stretching) appeared at 1398 and 1220 cm^{-1}. Besides, the sharp symmetric characteristic band at 673 cm^{-1} probably indicated silicate or amorphous glass.

Figure (10) Shows **a.** SEM microphotograph of a polycrystalline structure, **b.** EDX, **c.** XRD patterns of Egyptian blue minerals, **d.** ATR-FTIR spectrum of fragment painted with Egyptian blue.

3.2.3.2. *Egyptian green*
Egyptian green is a frit particle with sharp edges. SEM microphotograph displayed a polycrystalline structure, fig. (11-a). EDX analysis exhibited the main elements Cu, Ca, Si, and O, with Cl, fig. (11-b). According to the XRD spectrum, fig. (11-c), the main minerals were quartz (SiO_2), wollastonite (Ca, $Cu_3(Si_3O_9)$), and para-wollastonite ($CaSiO_3$). ATR-FTIR spectrum of Egyptian green, fig. (11-d) reported that the characteristic

bands at 1422 and 872cm^{-1} indicated C=O and C-O, respectively ascribable to calcite in green or plaster layer. In addition, the broad and strong characteristic bands at 1006 and 1002 cm^{-1}, respectively represented silicate O-Si-O. In addition, the amorphous silica showed at 782, 676, 798, 599, 552, and 462 cm^{-1}.
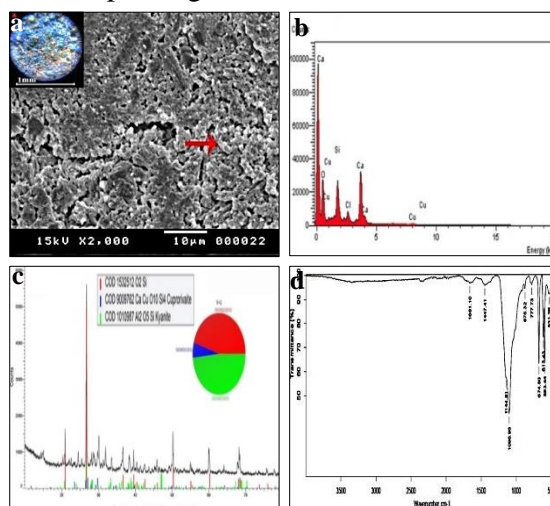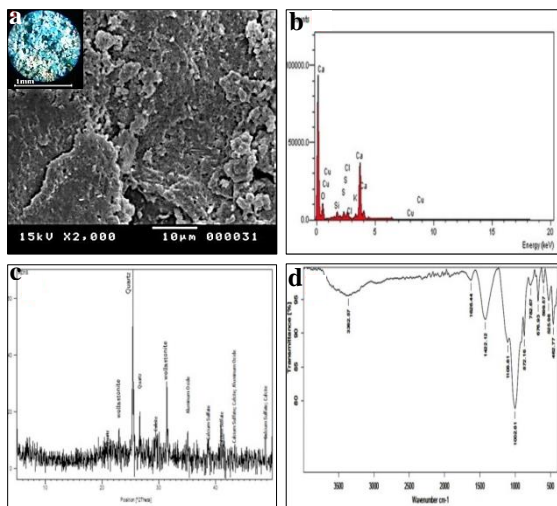

Figure (11) Shows **a.** SEM microphotograph of a poly-crystalline structure, **b.** EDX, **c.** XRD patterns of Egyptian green minerals, **d.** ATR-FTIR spectrum for fragment painted with Egyptian green.

3.2.3.3. *Red ochre*

Red ochre is composed of hematite Fe_2O_3 visible by optical microscopy in a brownish clayey matrix, usually coupled with clay minerals like kaolinite or Nacrite. SEM microphotograph, fig. (12-a) showed the hematite as sub-micrometric grains associated with platy grains of clay minerals. EDX analysis confirmed the presence of a high content of silicon and oxygen content; thus, the main elements of red ochre were Si, O, Fe, and Al with the presence of Na or K, fig. (12-b). XRD analysis, fig. (12-c) illustrated that the main minerals were quartz (SiO_2), hematite ($Fe_2 O_3$), and Nacrite as a clay mineral ($Al_2O_9Si_2$). In the ATR-FTIR spectrum, Fe-O appeared in the distinct bands at 671, 669, and 598 cm^{-1}. In addition, the characteristic broad bands at 1077 and 994

cm^{-1} could be attributed to (X–O–H bending, where X was most likely an octahedral ion −Al, Fe^{+2}, Fe^{+3}) as presented in fig. (12-d).

Figure (12) Shows **a.** SEM microphotograph of sub-micrometric grains, **b.** EDX, **c.** XRD patterns of red ochre, **d.** ATR-FTIR spectrum for fragment painted with red ochre.

3.2.3.4. *Yellow ochre*

Agglomerates of fine-grained were noticed under the optical microscope. Submicrometric grains were associated with platy grains of clay minerals, as noticed in the SEM microphotograph, fig. (13-a). EDX microanalysis, fig. (13-b) revealed that it was mainly composed of Si, O, Fe, and Al, referring to yellow ochre. XRD pattern, fig. (13-c) showed the main minerals, namely quartz (SiO_2), graphite (C), goethite (FeO_2), and Aluminosilicate material such as Nacrite ($Al_2O_9Si_2$). ATR-FTIR spectrum, fig. (13-d) revealed that the characteristic broadband of Si-O at 997 cm^{-1}, the sharp symmetric band at 670 cm^{-1}, and the characteristic peaks at 481 and 429 cm^{-1} were attributed to Fe-O.
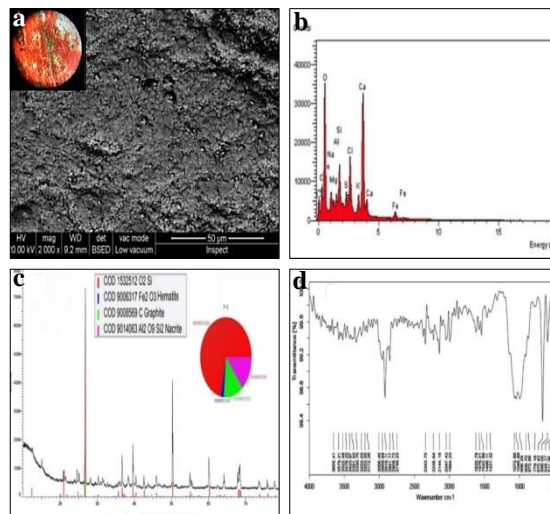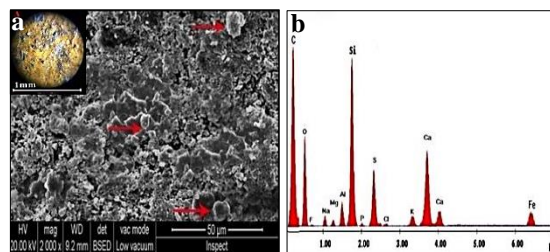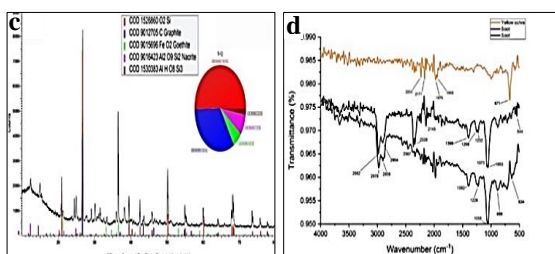
Figure (13) Shows **a.** SEM microphotograph of sub-micrometric grains, **b.** EDX, **c.** XRD patterns of yellow ochre, **d.** ATR-FTIR spectrum for fragment painted with yellow ochre.

4.2.4. Binding medium

According to the FTIR-ATR, the spectra presented to the numbers of painted surfaces mentioned above, the binding medium used in the Osiris chapel was *Arabic gum*, which composes of a hydrocolloid polysaccharide, carbohydrates, proteins, and some minerals like potassium and magnesium. *Arabic gum* was shown at the broad bands at 3446.2 and 3417.3 cm^{-1}. These bands were assigned to the functional group O-H characteristic of carbohydrates. The peaks in the range 2930-2900 cm^{-1} showed a C-H aliphatic asymmetrical stretching vibrational band, while the peak at 2860 cm^{-1} was the symmetrical stretching vibrational band. Besides, the absorption peaks at 1480-1300 cm^{-1} could be attributed to the binding band (C-H) and a binding band (C-O) 1300-900 cm^{-1}.

5. Discussion

Based on the above examinations and analyses, the Osiris chapel in Abydos was decorated with a group of decorations made with different methods and materials. The results of the present study are compatible with the results reported previously by many authors [2,3,12,13,39]. The investigations were utilized to answer some questions concerning materials and techniques used in this chapel. In addition to knowing how far from the surface, unwanted deposits, such as *soot* and *acrylic water proof* paint, penetrated the painted surface and how they affected it. Additionally, the study results

proved that the old Egyptian artesian used fine crystalline limestone composed mainly of calcite ($CaCO_3$), quartz (SiO_2), and traces from dolomite (ankerite Ca.$_{997}$(Mg.$_{273}$Fe.$_{676}$ Mn.$_{054}$) (CO_3)$_2$) to construct the walls of the chapel as attested previously by some authors [40,41]. Sandstone was used to construct the vaulted ceiling. It is composed mainly of quartz, anhydrite ($CaSO_4$), and kaolinite Al$_2$ (Si$_2$O$_5$)(OH)$_4$ [42-45]. Regarding the plaster layers on the sandstone, they were applied, while a very thin layer of gypsum ($CaSO_4$. $2H_2O$) was applied to the limestone. In some cases, the limestone was polished and colored directly without applying any plaster. The plaster layer consists of quartz, gypsum, anhydrite and calcite. In the same context, the pigments were identified as blue, green, red and yellow. The blue pigment (*Egyptian blue*) is the oldest synthetic pigment ever employed in human history [46]. It is multi-component synthetic pigment produced in ancient times since the 4th dynasty of the old kingdom in the 3rd millennium BC for tombs paintings and production of small objects [47]. It composed of $CaCuSi_4O_{10}$ (*Cuprorivaite*) [48], and it is known as calcium copper tetrasilicate or calcium copper phyllotetrasilicate [49]. This material was discovered by Cuprorivaite 1938 [50]. The producing of this material requires melting process of three initial components: **1)** *malachite* as copper-bearing ingredient, **2)** *quartz*, **3)** *lime* [51] in temperature rate between 850 and 950 °C, and it well decomposes above 1100 °C [52]. The green pigment (*Egyptian green*) is a turquoise mineral, which has the same chemical elements of Egyptian blue [53]. It was manufactured by a similar high temperature firing degree. The principal phase that creates this colour is a silica-rich, copper-containing glass [54]. It composed of quartz (SiO_2) and wollastonite, $CaSiO_3$ (Si_3O_9) or of para-wollastonite ($CaSiO_3$) as main minerals of wollastonite [55-58]. Their

ingredients are mixed in variable proportions (*with a higher amount of flux*) in temperature degree between 950-1150 °C for the Egyptian green [59]. This material (*wollastonite*) is mostly detected in mixtures containing a lower copper: calcium ratio; at higher temperature degrees [60]. This process that may be explained by the sintering reactions, which occur in a mixture of solid compounds during heat treatment [53]. *Red ocher* one of the most common pigments used in our region. It is the predominant red pigment throughout the history of ancient Egypt [61] it naturally occurring iron (III) oxide [62]. It consists mainly of quartz, hematite (Fe_2O_3), and nacrit (Al_2O_9 Si_2) as a clay mineral [63-68]. The pigment showed an important amount of iron by EDX and it had been confirmed by XRD analysis. In our study, hematite is the main crystalline phase in the red pigment, where, the atomic ratio between Fe and O is 2:3, which confirms that this particle correspond to (*fi*-Fe_2O_3) as attested by Ortega-Avilés, et al. [69] in his case study. The yellow pigment *(yellow ocher)* is a term used to describe pigments derived from weathered rock deposits containing varying proportions of the iron oxide hydroxide mineral goethite, together with quartz, clays, and other associated minerals [70]. It composed of goethite (FeO_2), graphite (C), nacrite (Al_2O_9 Si_2), [71]. It is considered one of the most common pigments of the major chromatic components of the famous four-colour palette [72]. In some cases, it was added to Egyptian blue to produce a bright lemon-yellow colour, which as it was used in west wall to distinguish part of Horus's kilt in the scene of the raising of the Djed pillar [73]. All the pigments were bound with a binding medium of *Arabic gum*, which revealed the composition of a hydrocolloid polysaccharide, carbohydrates, and proteins according to the FTIR-ATR spectra [40,66, 74-76]. From a specialized point of view,

the soot particles accumulated as a very thick layer on the ceiling resulting from the burning of candles and incense. These particles led to obscuring the details of the artistic and aesthetic values of these monuments by soiling [77]. In addition, they changed the water permeability properties of the original surface [26]. Soot contains acidic components that caused the decay of the stone. The effects of soot and other organic compounds form a suitable medium for SO_2 absorption from atmospheric increased by $CaSO_4$ [78]. On the other hand, the hydrophobic coatings that were commonly applied for the conserving and protecting the painted decorations during previous periods, over time, were degraded due to different external agents, such as AT, RH, salts, light, microorganisms, etc. [79-81]. Those agents can trigger multiple deterioration mechanisms, resulting in damage to one or more strata of the wall painting.

6. Conclusion

The results proved that the vaulted ceiling was made of sandstone. As for the walls, they were made of fine-crystalline limestone. The pigments were Egyptian blue, Egyptian green, red ocher, and yellow ochre. These pigments were mixed and bonded with Arabic gum as a binding medium. Moreover, the study monitored the effect of soot accumulated densely on the ceiling and tightly adhered to the walls despite its small amount, as it led to the obliteration of decorations and artistic and aesthetic landmarks, in addition to being an acidic environment that may lead to the formation of harmful acids and leads to more damage. Even more, the study found the harmful effect of hydrophobic coating applied during previous periods, namely their damaged, yellowish, and shiny unwanted appearance. In addition, they cracked and led to fluid retention, which in the presence of temperature and moisture, aggravating the situation. The study presented a documentation system via Photoshop and AutoCAD. Further investigations about utilizing cold atmospheric pressure plasma (CAP) to remove accumulated soot and aged coatings layers, in addition to decontaminating the painting surfaces against microorganisms shall be published.

References

[1] Baines, J. (1984). Abydos, temple of Sethos I: preliminary report. *The J. of Egyptian Archaeology*, Vol. 70 (1), pp. 13-22.

[2] Pavlidou, E., Mahmoud, H., Roumeli, E., et al. (2008). Identifying pigments in the temple of Seti I in Abydos (Egypt), in: Richter, S., Schwedt, A. (eds.) *EMC 2008 14th Euro. Microscopy Cong.*, Springer, Berlin, doi: 0.1007/978-3-540-85226-1_415.

[3] Helmi, F. & Attia, H. 1996). Characterization and conservation of Seti-I temple stone, Abydous, upper Egypt, in: Riederer, J. (ed.) *8th Int. Cong. on Deterioration and Conservation of Stone*, Möller Druck und Verlag Berlin, pp. 1123-1136

[4] O'Connor, D. (2009). *Abydos: Egypt's first pharaohs and the cult of Osiris*: Thames & Hudson, London.

[5] Sety, O. & El Zeini, H. (1981). *Abydos: Holy city of ancient Egypt*: LL Co., UK.

[6] Algernon, S. & Caulfeild, G. (1989). *The temple of the kings at Abydos. (Sety I.)*, Histories and Mysteries of Man, London.

[7] Al-Emam, E., Motawea, A. G., Janssens, K., et al. (2019). Evaluation of polyvinyl alcohol–borax/agarose (PVA–B/AG) blend hydrogels for removal of deteriorated consolidants from ancient Egyptian wall paintings, *Heritage Science*, Vol. 7 (22), doi: 10.1186/s40494-019-0264-z

[8] David, A. (2016). *Temple Ritual at Abydos*, The Egypt Exploration Society, London.

[9] Zayed, A. (1963). *Abydos*: US Government Printing Office, USA.

[10] Calverley, A., Broome, M., Gardiner, A., et al. (1933). *The temple of king Sethos I at Abydos*: Univ. of Chicago, USA.

[11] Wilkinson, R. (2000). *The complete temples of ancient Egypt*: Thames & Hudson, UK.

[12] Al-Emam, E., El-Gohary, M. & Abd EL Hady, M. (2014). Investigations of mural paintings of Seti I and Ramesses II tem-ples at Abydos-Egypt. *IJCS*, Vol. 5 (4), pp. 421-434

[13] Al-Emam, E., El-Gohary, M. & Abd El Hady, M. (2015). The paint layers of mural paintings at Abydos temples-Egypt: A closer look at the materials used. *MAA*, Vol.15 (3), pp. 113-121.

[14] El-Gohary, M. & Al-Naddaf, M. Characterization of brick used in the external casing of Roman bath walls "Gadara-Jordan", *MAA*, Vol. 9 (2), pp. 29-46

[15] Bityukova, L. & Limberg, M. (2005) Complex study of composition of building stones of the historical objects in Tallinn (Estonia) and assessment of stone deterioration on the base of geochemical data, *Geophysical Research Abstracts*, Vol. 7, pp. 1-4

[16] Ignatavičius, Č. & Ignatavičius, G. (2005) Investigation of damage and microclimate deterioration caused by dampness in the palace of signatories to the declaration of independence, *Indoor and Built Environment*, Vol. 14 (1), pp. 89-95

[17] El-Gohary, M. & Abdel Moneim A. (2021). The environmental factors affecting the archaeological buildings in Egypt, "II deterioration by severe human activities", *Periodico di Mineralogia*, Vol. 90, pp. 261-275

[18] Kamil, J. (2012). *Christianity in the land of the pharaohs: The Coptic Orthodox Church*: Routledge, UK.

[19] Roberts, B. (1988). An account of the conservation and preservation procedures following a fire at the huntington lffirary and art gallery. JAIC, Vol. 27 (1), pp. 1-31.

[20] Spafford-Ricci, S. & Graham, F. (2000). The fire at the royal Saskatchewan museum, part 1: salvage, initial response, and the implications for disaster planning, JAIC, Vol. 39 (1), pp. 15-36.

[21] Spafford-Ricci, S. & Graham, F. (2000). The fire at the royal Saskatchewan museum, part 2: removal of soot from artifacts and recovery of the building. JAIC, Vol. 39 (1), pp. 37-56.

[22] Heydenreich, G. (2004). Fire, water, air: more than 1000 square metres of soiled surfaces to be cleaned. *CR Interdisciplinair Vakblad Voor Conservering en Restauratie*, Vol. 5 (3), 20-21, pp. 23-29.

[23] Tsang, J-S. & Babo, S. (2011). Soot rem-oval from acrylic emulsion paint test panels: A study of dry and non-contact cleaning, in: ICOM-CC (ed.) *16th Triennial Conference*, Lisbon, pp. 1-9

[24] Mašková, L., Smolík, J., Ondráček, J., et al. (2020). Air quality in archives housed in historic buildings: Assessment of concentration of indoor particles of outdoor origin. *Building and Environment*, Vol. 180, doi: 10.1016/j.buildenv. 2020.107024

[25] Bellan, L., Salmon, L. & Cass, G. R. (2000). A study on the human ability to detect soot deposition onto works of art. *Environmental Science & Technology*, Vol. 34 (10), pp. 1946-1952.

[26] El Bana, S., Shoeab, A. & dam, Kh (2016). Project TT 110 (Tomb of Dje-huty), https://edit.gerda-henkel-stiftung. de/ctt/symposium2016/conservation-pr oject-tt-110-tomb-of-djehuty_100458.h tml (10-5-2022).

[27] Van Grieken, R., Delalieux, F. & Gysels, K. (1998). Cultural heritage and the environment. *Pure and Applied Chemistry*, Vol. 70 (12), pp. 2327-2331.

[28] Lazzari, M. & Chiantore, O. (2000). Thermal-ageing of paraloid acrylic protective polymers, *Polymer*, Vol. 41 (17), pp. 6447-6455.

[29] Feller, R. (1963). New solvent type varnishes, in: Thompson, G. (ed.) Recent *Advances in Conservation Conf.*, Butterworths, London, pp. 171-175.

[30] Brendley, W. & Bakule, R. (1985). Chemistry and technology of acrylic resins for coatings, in: Tess, R. & Poehlein, G. (eds.) *Applied Polymer Science*, American Chemical Society, Washington DC, pp. 1032-1052

[31] Villiunaite, I. (2016). *Polymeric dispersions for the protection of limestone: application on noto and comiso stone*, ARCHM, Facoltà di Scienze Matematiche, Fisiche e Naturali, Sapienza, Univ., Italy.

[32] Baglioni, P., Giorgi, R. & Chelazzi, D. (2016). The degradation of wall paintings and stone: specific ion effects. *Current Opinion in Colloid & Interface Science*, Vol.23, pp. 66-71.

[33] Al-Emam, E., Motawea, A., Caen, J., et al. (2021). Soot removal from ancient Egyptian complex painted surfaces using a double network gel: empirical tests on the ceiling of the sanctuary of Osiris in the temple of Seti I—Abydos, *Heritage Science*, Vol. 9 (1), doi. 10.11 86/s40494-020-00473-1

[34] Tabasso, M. (1995). Acrylic polymers for the conservation of stone: Advantages and drawbacks. *APT Bulletin*: *J. of Preservation Technology*, Vol. 26 (4), pp. 17-21.

[35] Zhang, H., Liu, Q., Liu, T., et al. & (2013). The preservation damage of hydrophobic polymer coating materials in conservation of stone relics. *Progress in Organic Coatings*, Vol. 76 (7-8), pp. 1127-1134

[36] El-Gohary, M. (2015). Methodological evaluation of some consolidants interference with ancient Egyptian sandstone "Edfu mammisi as a case study", *Progress in Organic Coatings*, Vol. 80. pp. 87-97

[37] Margariti, C. (2019). The application of FTIR microspectroscopy in a non-invasive and non-destructive way to the study and conservation of mineralised excavated textiles, *Heritage Science*, Vol.7(1),doi.org/10.1186/s40494-019-0304-8

[38] Bitossi, G., Giorgi, R., Mauro, M., et al. (2005). Spectroscopic techniques in cultural heritage conservation: A survey. *Applied Spectroscopy Reviews*, Vol. 40 (3), pp. 187-228.

[39] Mahmoud, H. & Papadopoulou, L. (2013). Archaeometric analysis of pigments from the tomb of Nakht-Djehuty (TT189), El-Qurna necropolis, Upper Egypt. *ArcheoSciences*, Vol. (37), pp. 19-33.

[40] Derrick, M., Stulik, D. & Landry, J. (2000). *Infrared spectroscopy in conservation science*: Getty Pub, USA.

[41] Reig, F., Adelantado, J., & Moreno, M. (2002). FTIR quantitative analysis of calcium carbonate (calcite) and silica (quartz) mixtures using the constant ratio method: Application to geological samples, *Talanta*, Vol. 58 (4), pp. 811-821.

[42] Hosam, I., & Kamh, G. (2016). Quantification of salt weathering at hot deserts and evaluation of reconstruction rock, Hibis temple, Kharga oasis, western desert, Egypt. *J. of Arid Land Studies*, Vol. 26 (3), doi: 10.14976/jals.26.3_143.

[43] Ojima, J. (2003). Determining of crystalline silica in respirable dust samples by infrared spectrophotometry in the presence of interferences. *J. of Occupational Health*, Vol. 45 (2), pp. 94-103.

[44] Meftah, N., & Mahboub, M. (2020). Spectroscopic characterizations of sand dunes minerals of El-Oued (Northeast Algerian Sahara) by FTIR, XRF and XRD analyses, *Silicon*, Vol.12 (1), pp. 147-153.

[45] Medini, H. & Arbi, M. (2018). Chemical and physical analysis of sandstone and relationship with weathering damage of Madâin Sâlih monuments, *J. of Taibah Univ. for Science*, Vol. 12 (1), pp. 37-45.

[46] Baraldi, P., Bondioli, F., Fagnano, C., et al. (2001). Study of the vibrational spectrum of cuprorivaite, *Ann. Chim.*, Vol. 91 (11-12), pp. 679-692.

[47] Ingo, G., Çilingiroglu, A., Di Carlo, G., et al. (2013). Egyptian blue cakes from the Ayanis fortress (Eastern Anatolia, Turkey): micro-chemical and -structural investigations for the identification of manufacturing process and provenance, *J. of Archaeological Science* Vol. 40, pp. 4283-4290.

[48] Jaksch, H., Seipel, W., Weiner, K., et al. (1983). Egyptian blue-cuprorivaite a window to ancient Egyptian technology, *Die Naturwissenschaften*, Vol. 70, pp. 525-535.

[49] Pisareva, S., Shibanova, I., Kadikova, I. (2021). Identification of $CaCuSi_4O_{10}$ (Egyptian blue) in the "Birch. Spring" painting by Robert Falk (1907) using photoluminescence, *J. of Cultural Heritag*e, Vol. 50, pp. 126-138

[50] Cuprorivaite, M. (1938). Un nuovo minerale, *Periodico di Mineralogia*, Vol. 8, pp. 333-345.

[51] Tite, M., Bimson, M. & Cowell, M. (1984). Technological examination of Egyptian blue, in: Ambert, J. (ed.) *Archaeological Chemistry III*, Advances in Chemistry 205, American Chemical Society, Washington D.C, pp. 215-42.

[52] Hatton, G., Shortland. A. & Tite, M. (2008). The production technology of Egyptian blue and green frits from second millennium BC Egypt and Mesopotamia, *J. of Archaeological Science*, Vol. 35 (6), pp. 1591-1604

[53] Pagès-Camagna, S. & Colinart, S. (2003). The Egyptian green pigment: Its manufacturing process and links to Egyptian blue, *Archaeometry*, Vol. 45 (4), pp. 637-658.

[54] Hallmann, A., Rickerby, S. & Shekede, L. (2021). Blue and green in the décoration of a Kushite chapel in Karnak, Egypt: Technical evaluation using low-tech, non-invasive procedures, J. of *Archaeological Science Reports*, Vol. 39, doi: 10.1016/j.jasrep.2021. 103190.

[55] Panagopoulou, A., Karanasios, K., & Xanthopoulou, G. (2016). Ancient Egy-

ptian Blue ($CaCuSi_4O1_0$) pigment by modern solution combustion synthesis method, *Eurasian Chemico Technological J.*, Vol. 18 (1), pp. 31-37.

[56] Lucas, A. & Harris, J. (2011). *Ancient Egyptian materials and industries*, 4th ed., Dover Pub., USA.

[57] Moussa, A. (2013). Comparative study of Egyptian blue fragments from Egypt and Tunisia, *EJARS*, Vol. 3 (1), pp. 13-19.

[58] Marshall, L-J., Williams, J., Almond, M., et al. (2005). Analysis of ochers from Clearwell caves: the role of particle size in determining colour. *Spectrochimica Acta Part A: Molecular and Biomolecular Spectroscopy*, Vol. 61 (1-2), pp. 233-241.

[59] Bloise, S., Abd El Salam, R., De Luca, G., et al. (2016). Flux growth and characterization of cuprorivaite: The influence of temperature, flux, and silica source, *Appl. Phys. A: Mater. Sci. Process.*, Vol. 122, pp. 1-8.

[60] Obeid, M. (2014). Crystallization of synthetic wollastonite prepared from local raw materials, *Int. J. of Materials and Chemistry*, Vol. 4 (4), pp.79-87

[61] Hedegaard, S., Delbey, T., Brøns, C., et al. (2019). Painting the palace of Apries II: Ancient pigments of the reliefs from the palace of Apries, lower Egypt, *Heritage Science*, Vol. 7, doi: 10.1186/ s40494-019-0296-4

[62] Fulcher, K., Stacey, R. & Spencer, N. (2020). Bitumen from the Dead Sea in early Iron age Nubia. *Scientific Reports*, Vol. 10, doi: 830910.1038/s41598-020-64 209-8

[63] Mahmoud, H. (2014). Investigations by Raman microscopy, ESEM and FTIR-ATR of wall paintings from Qasr el-Ghuieta temple, Kharga Oasis, Egypt, *Heritage Science*, Vol. 2 (1), doi: 10.11 86/s40494-014-0018-x.

[64] Zagora, J. (2013). SEM-EDX pigment analysis and multi-analytical study of the ground and paint layers of Francesco Fedrigazzi's painting from Kostanje, CeROArt Online, EGG 3, *http://ceroart. revues.org/3248* (11-12-2022).

[65] Abdrabou, A., Abdallah, M. & Kamal, H. (2017). Scientific investigation by technical photography, OM, ESEM, XRF, XRD and FTIR of an ancient Egyptian polychrome wooden coffin, *Conservar Património*, Vol. (26), pp. 51-63.

[66] Čiuladienė, A., Luckutė, A., Kiuberis, J., et al. (2018). Investigation of the chemical composition of red pigments and binding media, *Chemija*, Vol. 29 (4), doi: 10.6001/chemija.v29i4.3840

[67] Rosso, D., Martí, A. & d'Errico, F. (2016). Middle stone age ochre processing and behavioural complexity in the horn of Africa: Evidence from Porc-Epic cave, Dire Dawa, Ethiopia. *PloS one*, Vol. 11 (11), doi: 10.1371/ journal.pone.0164793.

[68] Veneranda, M. (2017). *Development of novel procedures for the preservation of archaeological irons and mural paintings*, Ph.D., Analytical Chemistry dept., Universidad del Pais Vasco, Spain.

[69] Ortega-Avilés, M., San-Germáan, C. & Mendoza-Anaya, D. (2001). Characterization of mural paintings from Cacaxtla, *J. of Matreials Science*, Vol. 36, pp. 2227-2236

[70] Eastaugh, N., Walsh, V., Chaplin, T., et al. (2008). *Pigment compendium: A dictionary and optical microscopy of historical pigments*, Butterworth- Oxford.

[71] Helwig, K. (1998) The characterisation of iron earth pigments using infrared spect-roscopy, in: IRUG & Pretzel, B. (eds.) The Second Infrared and Raman User's Group (IRUG 2) Conf., Victoria and Albert Museum, London, UK, pp. 83-92.

[72] Perdikatsis, V. (2008). The use of red and yellow ochres as painting materials

in ancient Macedonia, in: Facorellis, Y., Zacharias, N. & Polikreti, K (eds.) *4th Symp. of the Hellenic Society for Archaeometry*, Archaeopress, UK, pp. 559-567

[73] Coulon, L. (2012). Le temple de Karnak, lieu de gu´erison: A` propos d'une chapelle kouchite dédiée á Osiris sauveur, Égypte, *Afrique et Orient*, Vol. 67, pp. 49-58.

[74] Elnour, A., Mirghani, M., Kabbashi, N., et al. (2019). Active fractions of methanol crude obtained from Acacia seyal gum: antioxidant capacity using FTIR analysis. *Borneo J. of Pharmacy*, Vol. 2 (2), pp. 94-107.

[75] Daoub, R., Elmubarak, A., Misran, M., et al. (2018). Characterization and functional properties of some natural Acacia gums. *J. of the Saudi Society of Agricultural Sciences*, Vol.17 (3), pp. 241-249.

[76] Fathihah, M., & Khairunnisa, M. (2021). Characteristics and carbon dioxide adsorption performance of candle soot-activated by potassium hydroxide, *IOP Conf. Series: Earth and Environmental Science*, doi: 10.1088/1755-1315/765/ 1/012087.

[77] El-Gohary, M. (2010). Investigation on limestone weathering of El-Tuba minaret El-Mahalla, Egypt: A case study, *MAA*, Vol. 10 (1), pp. 61-79.

[78] El-Gohary, M. (2008). Air pollution and aspects of degradation "Umayyad liwãn-Amman citadel as a case study", *Int. J. of Applied Sciences Research*, Vol. 4 (6), pp. 669-682

[79] Abdel-Ghani, M. & Mahmoud, M. (2013). Spetroscopic investigation on paint layer of Sabil-Kuttab Umm Abbas ceilling, Mohamed Ali era in Cairo, Egypt: Identification of unusual paintings and medium, *EJARS*, Vol. 3 (2), pp. 95-105

[80] El-Gohary, M. & Abo El-Magd, M. (2018). Influence of acrylic coatings and nanomaterials on the interfacial, physical, and mechanical properties of limestone-based monuments "Amenemhat II temple as a case study", *IJCS*, Vol. 9 (2), pp. 219-234

[81] Ciferri, O. (1999). Microbial degradation of paintings, *Appl. Environ Microbiol.*, Vol. 65 (3), pp. 879-885.